Covalent Immobilization of Polyoxotungstate on Alumina and Its Catalytic Generation of Sulfoxides

Lanlan Hong, Pyaesone Win, Xuan Zhang, Wei Chen,* Haralampos N. Miras and Yu-Fei Song*

State Key Laboratory of Chemical Resource Engineering, Beijing University of Chemical Technology, Beijing 100029, P. R. China. Email: songyufei@hotmail.com or songyf@mail.buct.edu.cn

Abstract: Structural and chemical stability of the immobilized polyoxometalates (POMs)-containing catalysts is one crucial factor for their industrial application. In this work, we discuss the preparation of a novel $P_2W_{15}@Al_2O_3$ catalyst using a facile condensation reaction between the tri-lacunary POM of $Na_{12}[\alpha\text{-}P_2W_{15}O_{56}]\cdot 24H_2O$ (P_2W_{15}) and the hydroxyl groups on the surface of the spherical $\gamma\text{-}Al_2O_3$ under acidic conditions. The heterogeneous catalyst was characterized by the ^{31}P NMR, FT-IR, XRD, XPS, TG, Raman, HR-TEM and BET. The $P_2W_{15}@Al_2O_3$ catalyst showed excellent stability, highly efficient reactivity and selectivity for the oxygenation of thioethers to sulfoxides which are a very useful intermediate in organic synthesis and industrial preparation of drugs. The catalyst could be recycled and reused at least ten times without any observable loss of its catalytic efficiency, mainly due to the covalently grafted $\{P_2W_{15}\}$ cluster and high dispersion onto the $\gamma\text{-}Al_2O_3$ surface.

Polyoxometalates (POMs) are a class of discrete anionic metal-oxides of V, Mo, W and Nb *etc*.[1] in their highest oxidation states exhibiting unrivalled structural archetypes as well as a wide range of sizes, unique physical properties[2] and applications[3] in areas as diverse as catalysis, medicine, electrochemistry, photochromism and magnetism etc.[4] Additionally, their solution processability due to their high solubility[1] and low lattice energies[2] due to generally weak interactions between the POMs clusters and the associated counterions (NH_4^+, K^+, Na^+ etc), render them ideal candidates and useful components for the design of functional materials such as catalysts. More specifically, studies on POM-based catalysis are mainly focused on the design of simplified routes for the preparation of heterogeneous systems due to catalyst recoverability,

reusability and excellent chemical, structural and thermal-stability.[3]

Immobilization and solidification of POM species on various substrates are two widely applied approaches for the generation of multifunctional POM-based heterogeneous catalysts.[3,4] Despite great efforts have been made for the efficient immobilization of POMs on supports such as SiO_2,[5] Al_2O_3,[6] ZrO_2,[7] zeolites[8] and activated carbon[9] materials, the produced composite materials generally suffer from various issues that need to be taken into consideration. For example, heterogeneous catalysts based on the electrostatic interactions developed between the POM species and the supports suffer from stability issues due to POM leaching.[10-12] In the case of the heterogeneous catalysts produced under high temperature regimes (eg. calcination) usually leads to structural rearrangements and finally the compromise of the POMs' structural integrity which greatly limits the offered opportunities to exploit the wide range of functionalities directly correlated to the POMs' structural features.[6,13,14] Therefore, utilization of robust support surfaces which preserve the POM's structural integrity for the development of heterogeneous catalysts for a wide range of processes, is highly desirable.

Alumina-based particles exhibit remarkable properties, such as well-defined pore structure and high specific surface areas. The spherical γ-Al_2O_3 exhibits good physical stability, high crush strength and great controllability. For these reasons, it is widely employed in the chemical and petrochemical industries.[15-22] In this paper, we report the preparation of the P_2W_{15}@Al_2O_3 composite material by immobilization of POMs onto spherical γ-Al_2O_3 particles (Scheme 1) and we discuss its catalytic efficacy for the oxygenation of thioethers.

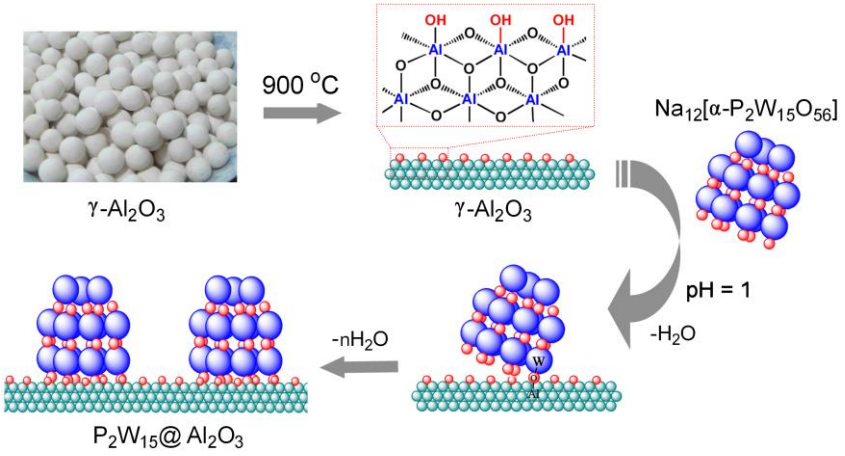

Scheme 1. The synthetic process of P_2W_{15}@Al_2O_3.

Results

The $P_2W_{15}@Al_2O_3$ composite material was synthesized by immobilization of $Na_{12}[\alpha\text{-}P_2W_{15}O_{56}]\cdot 24H_2O$ clusters onto the surface of the spherical $\gamma\text{-}Al_2O_3$ particles under acidic conditions.[23,24] In an effort to optimize the immobilization conditions, we immobilized the POM clusters under various pH conditions ranging from 6 to 1 (Figure 1). The resultant solid was separated from the reaction mixture by filtration and washed with 0.3 M LiCl solution to remove the physically adsorbed $\{P_2W_{15}\}$ clusters.[25]

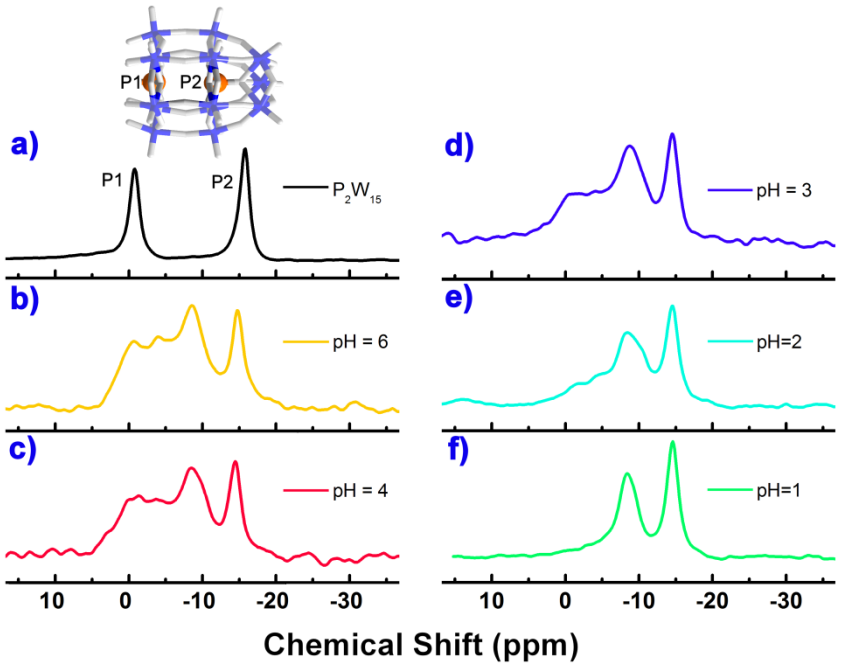

Figure 1. Solid state ^{31}P NMR of (a) $Na_{12}[\alpha\text{-}P_2W_{15}O_{56}]\cdot 24H_2O$ and (b-f) $P_2W_{15}@Al_2O_3$ composite material prepared under different pH environments.

Figure 1a shows the solid state ^{31}P NMR spectra of $Na_{12}[\alpha\text{-}P_2W_{15}O_{56}]\cdot 24H_2O$, where the two observed signals located at -0.79 ppm and -15.77 ppm can be assigned to the non-equivalent phosphorus atoms, P1 and P2, respectively.[26] Upon decrease of the pH value from 6 to 1, the left shoulder peak centered at -0.79 ppm decreases and splits into several peaks in the range of -0.79 to -8.41 ppm, which is a potential indication of partial decomposition at specific pH values of the cluster prior to immobilization on the alumina surface. On the other hand, the signal located at -15.77 ppm, shifts gradually to -14.58 ppm due to the reaction between the $\{P_2W_{15}\}$ anions and the $\gamma\text{-}Al_2O_3$ surface. According to the results obtained by the solid state ^{31}P NMR, the optimum

conditions for the effective immobilization of the lacunary Dawson anions onto the alumina support takes place at pH = 1. This is in agreement with the Mulcahy's report,[23] where the positive net surface charge acquired at pH values below the isoelectric point (IEP) of the support, attracts and stabilizes the anionic species from the bulk solution. However, a simple electrostatic model cannot account for the adsorption of theses anions. It is suggested that this is a two-step process where the electrostatic ion pairing occurs first as soon as the pH value is below the IEP = 8.6 of γ-Al_2O_3 (Figure S1), followed by a condensation reaction between the $\{P_2W_{15}\}$ anions and the γ-Al_2O_3 surface according to the following equations:

$$Al - OH_2^+ + P_2W_{15}O_{56}^{12-} \rightleftharpoons Al - OH_2^+P_2W_{15}O_{56}^{12-} \quad (1)$$

$$Al - OH_2^+P_2W_{15}O_{56}^{12-} \rightleftharpoons Al - O - P_2W_{15}O_{55}^{11-} + H_2O \quad (2)$$

The W=O and W-O stretching and bending vibrations of the P_2W_{15} generally occur below 1000 cm^{-1} thus it is difficult to detect them by Fourier transform-infrared (FT-IR) due to the strong IR absorption of the γ-Al_2O_3 supports in this region (Figure S2).[13,27] The XRD pattern of the P_2W_{15}@Al_2O_3 composite is similar to that of Al_2O_3, indicating no diffraction of the $Na_{12}[\alpha\text{-}P_2W_{15}O_{56}]\cdot 24H_2O$ due to poor crystallinity and co-existence of other crystalline phases (Figure S3). The Raman spectra of the P_2W_{15}@Al_2O_3 are presented in Figure 2a. It can be seen that the γ-Al_2O_3 support is not Raman active, allowing detection of all the W-O vibrations.[28] The characteristic vibrations of bulk $\{P_2W_{15}\}$ are located at 955, 871 and 827 cm^{-1}, respectively. The P_2W_{15}@Al_2O_3 exhibit Raman bands located at 980, 909 and 839 cm^{-1}, respectively, which can be assigned to the W=O stretch bands and W-O-W stretch modes of the immobilized cluster.[29] The Raman shifts are due to the strong interactions between the tri-lacunary POM cluster and the γ-Al_2O_3 support, leading to the decrease of the cluster's and/or the alumina's local symmetry.[30]

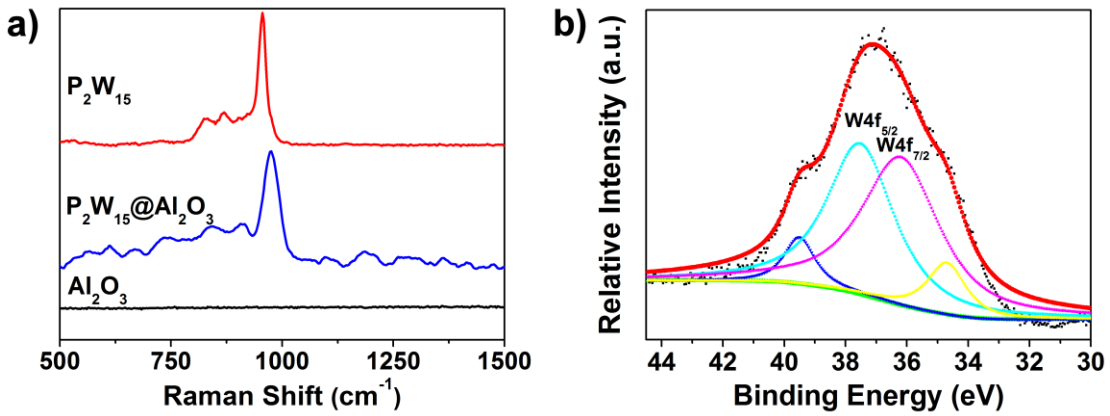

Figure 2. (a) Raman spectra of Al_2O_3, $P_2W_{15}@Al_2O_3$ and P_2W_{15}, respectively; (b) W_{4f} XPS spectrum of $P_2W_{15}@Al_2O_3$.

Additionally, XPS spectroscopy was used in order to determine the oxidaiton centres of metal centres. More specifically, the XPS spectrum for W_{4f} (Figure 2b) revealed two peaks located at 34.8[31], 36.2[32] eV in the energy region of $W4f_{7/2}$, 37.5, 39.5 eV[33,34] in the energy region of $W4f_{5/2}$, which are consistent with the W^{VI} oxidation state. The thermogravimetric study of the $P_2W_{15}@Al_2O_3$ composite (see Figure S4) performed under nitrogen in the temperature range of 25 to 800 ^oC and revealed two main weight losses. The first one of 1.9% ranging from 25 to 207 ^oC can be attributed to the loss of the absorbed water and crystallization water molecules of the sample. The second weight loss of 1.4 % between 207 and 523 ^oC can be assigned to the loss of the constitutional water from $P_2W_{15}@Al_2O_3$.[35]

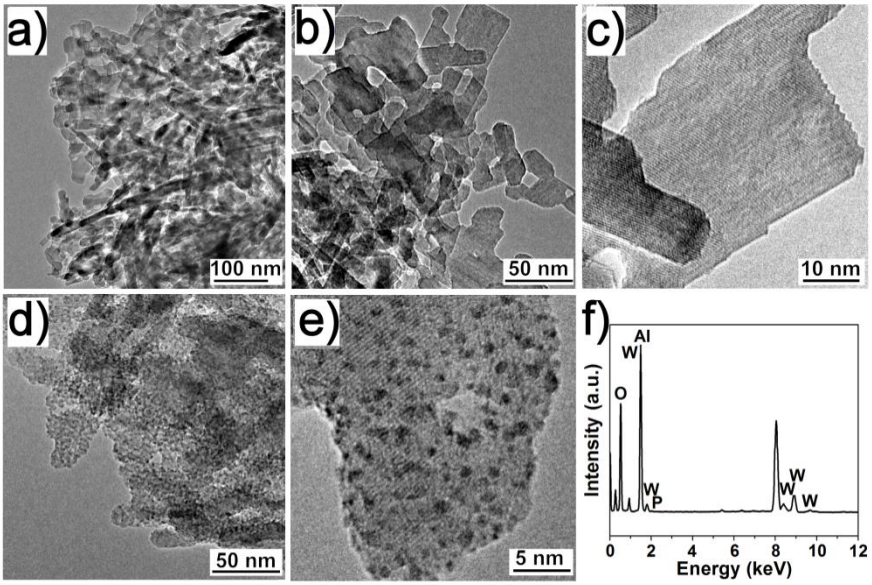

Figure 3. High-resolution-TEM images of Al_2O_3 (a-c) and $P_2W_{15}@Al_2O_3$ (d-e), respectively. f)

Energy dispersive spectroscopy of $P_2W_{15}@Al_2O_3$.

SEM images of the $P_2W_{15}@Al_2O_3$ composite material show sheet-like morphologies that are similar to that of the bare Al_2O_3 support (Fig. S5-S6). The HRTEM images of the $P_2W_{15}@Al_2O_3$ composite material revealed unambiguously the presence of $\{P_2W_{15}\}$ clusters on the γ-Al_2O_3 support, in the form of dark dots of 1~2 nm size (Figure 3). In order to confirm further the covalent linkage between the $\{P_2W_{15}\}$ clusters and the γ-Al_2O_3 support, we studied the stability of the $P_2W_{15}@Al_2O_3$ composite in LiCl solution, according to previously reported procedure.[13] The $P_2W_{15}@Al_2O_3$ composite materials were dispersed in 0.3 M LiCl solution under vigorous stirring for 12 h, the solution was filtered and dried under vacuum. The procedure repeated three times; close examination of the HRTEM images (Fig S7) obtained from the collected and dried material showed that the POM clusters remained immobilized on the surface of γ-Al_2O_3 whilst ICP analysis on the collected filtrates showed that no W element was present. The experimental data strongly suggest that the $\{P_2W_{15}\}$ clusters are not just physically adsorbed on the γ-Al_2O_3 since the presence of Li^+ counterions would have removed the clusters from the surface and extracted them into the solution. Examination of the elemental composition of the material by energy dispersive spectroscopy (EDS) showed that P and W atoms are present on the $P_2W_{15}@Al_2O_3$ composite material (Fig 3f) whilst X-ray fluorescence spectroscopy revealed that the loading of $\{P_2W_{15}\}$ on the γ-Al_2O_3 support is approximately 9.98%.

As shown in Figure 4 and Table S1, the N_2 adsorption-desorption isotherms of γ-Al_2O_3 and $P_2W_{15}@Al_2O_3$ are classified as type IV with a clear H1-type hysteresis loop according to the IUPAC classification, indicating the presence of meso-porosity. The pore size distribution curves of γ-Al_2O_3 and $P_2W_{15}@Al_2O_3$ found to be 42.74 and 30.93 nm, respectively, indicating that the regular meso-porous channels of the γ-Al_2O_3 support are retained in the corresponding $P_2W_{15}@Al_2O_3$ catalysts. The pore size distribution curves of the $P_2W_{15}@Al_2O_3$ reduced with the P_2W_{15} loading which can be explained by the fact that the pores are partially blocked by $\{P_2W_{15}\}$ clusters.

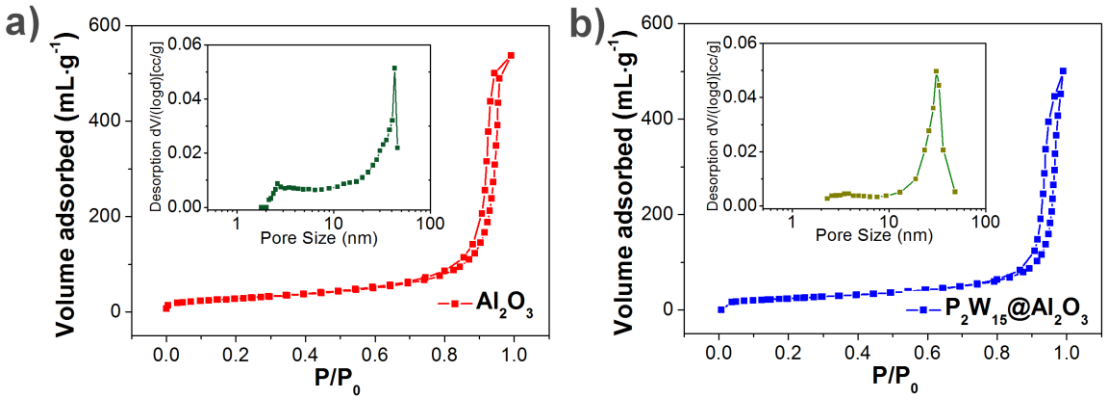

Figure 4. The N_2 adsorption-desorption isotherm and the pore size distribution of (a) Al_2O_3, (b) P_2W_{15}@Al_2O_3.

Catalytic activity.

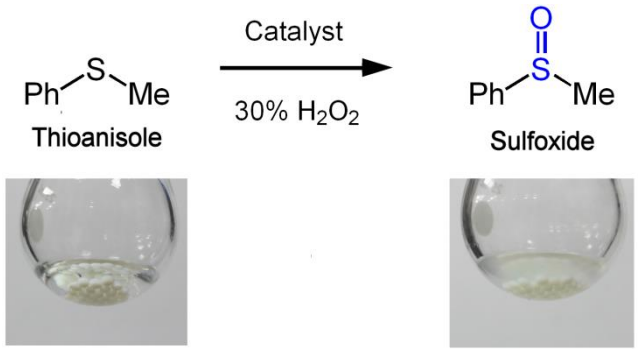

Scheme 2. Selective oxidation of sulfides to sulfoxides by using the P_2W_{15}@Al_2O_3 composite materials.

Catalytic oxidations of organic compounds under mild conditions are of both considerable intellectual interest and potential utility.[36,37] Catalytic oxidation of organic sulfides remains a topical interest due to the versatile utility of both sulfoxides and sulfones in organic synthesis.[38-40] While a mass of oxygen donors are available, utilization of H_2O_2 as "green" oxygen donor has become increasingly prominent.[41-44] In this work, catalytic oxidation of thioanisole in the presence of P_2W_{15}@Al_2O_3 as catalyst and H_2O_2 as oxidant has been carried out (Scheme 2). The selectivity of sulfoxide products and the conversion of the initial sulfides have been quantified using gas chromatography (GC) (Figure S8, S9) and ^{1}H.NMR of the reactant (thioanisole) and the product upon completion of the reaction (Figure 5). Table S2 summarizes the reactivity data for the oxidation of thioanisole in CH_3OH at 25 ^{o}C in the presence of the {P_2W_{15}}, P_2W_{15}@Al_2O_3 and in

the absence of the $P_2W_{15}@Al_2O_3$. In the presence of the $P_2W_{15}@Al_2O_3$ as a catalyst, the conversion and selectivity were improved considerably. This indicates that the $P_2W_{15}@Al_2O_3$ is an effective catalyst for the oxygenation of thioanisole by H_2O_2. In an effort to optimize the reaction conditions, various solvents, reaction times, amounts of H_2O_2 and catalyst were investigated (Figure S10-S12, and Table S3). The determined optimal conditions found to be the following: thioanisole = 1 mmol, H_2O_2 = 82 μL, CH_3OH = 200 μL. Thus, the experiments for the determination of the kinetic parameters for the catalytic oxidation of thioanisole, were carried out using the optimized conditions.

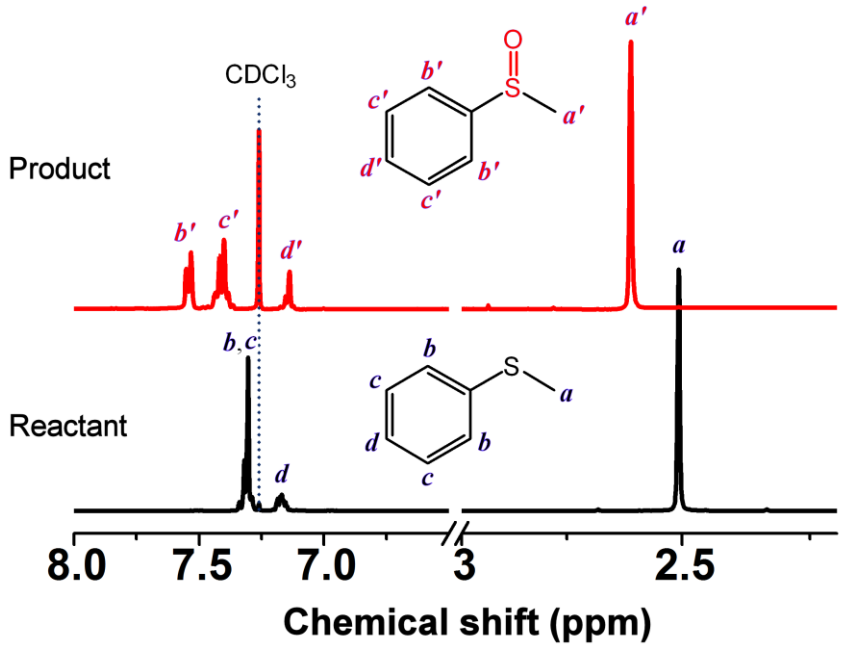

Figure 5. ^1H NMR ($CDCl_3$) spectra of the reactant (thioanisole) and the product (sulfoxide). Experimental conditions: thioanisole = 1 mmol, H_2O_2 = 1 mmol, catalyst = 2.5 μmol, CH_3OH = 200 μL, T=25 °C, *t* = 35 min.

Reaction kinetics for the oxidation of thioanisole are presented in Figure 6, where the (C_t/C_0) is plotted against the reaction time. The C_0 and C_t are the initial thioanisole concentration and thioanisole concentration at time t, respectively. The rate constant *k* of the oxidation reaction is determined to be -0.082 min^{-1} on the basis of Equations (1) and (2). The oxidation of thioanisole and subsequent conversion to the product (sulfoxide) can be completed in about 35 min.

$$\frac{-dC_t}{dt} = kC_t \quad (1)$$

$$\ln\frac{C_0}{C_t} = kt \qquad (2)$$

As such, the catalyst shows high catalytic efficiency for the oxidation of sulfides to sulfoxides, and the catalytic reaction exhibits pseudo-first-order kinetics for the oxidation of thioanisole with a 99 % selectivity for sulfoxides (R^2 = 0.99). In an effort to confirm that the catalyst is truly heterogeneous, we removed the catalyst from the reaction mixture when the conversion reached a value of 60 % after 15 min. Real time monitoring of the reaction mixture by GC showed that the substrate catalytic conversion stopped immediately. The addition of the catalyst back to the reaction mixture restarted the reaction as shown in Figure S13.

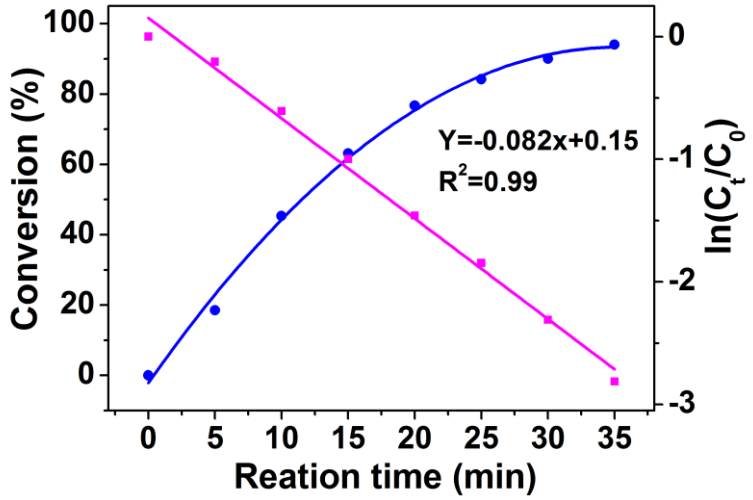

Figure 6. The catalytic conversion of thioanisole and ln (C_t/C_0) as functions of reaction time. Reaction conditions: thioanisole = 1 mmol, H_2O_2 = 1mmol, CH_3OH = 200 μL, T = r.t., *t* = 35 min.

After confirming the stability and efficiency of the composite material we investigated the general applicability and selectivity of the as-prepared catalyst of P_2W_{15}@Al_2O_3, we utilized a series of thioether-based compounds as substrates in catalytic oxygenation reactions under the same conditions (Table 1). The results revealed that alkyl-aryl thioethers and 4-Pentamethylene sulfides can be selectively fully converted to the desired product. However, 2-Bromothioanisole showed a relatively low conversion, which might be due to increased steric hindrance and/or electrophilic effect (Entry 4). Interestingly, the phenylallyl thioether gave a conversion of 63% to the desired sulfoxide along with an unknown by-product (Entry 6).

Table 1 Oxidation of various sulfides to the corresponding sulfoxides by using 30% H_2O_2 and $P_2W_{15}@Al_2O_3$.

Entry	Substrate	Product	Convers.[a] /%	Sel.[b] /%
1	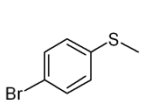	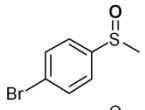	94	97
2	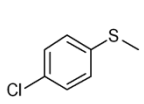	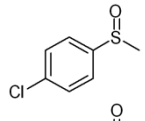	90	99
3	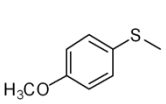	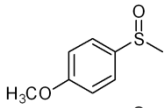	98	97
4	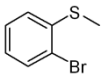	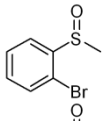	34	100
5	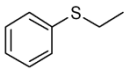	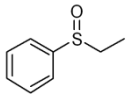	94	97
6	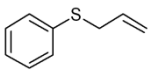	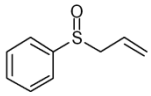	63	92
7			96	91

Experimental conditions: substrate = 1 mmol, H_2O_2 = 1 mmol, catalyst = 2.5 μmol, CH_3OH = 200 μL, T=25 °C, *t* = 35 min.

The main advantage of using heterogeneous catalysts in a liquid-phase reaction is the ease of separation and recycling of the catalyst. In order to confirm in our case that there are no catalyst leaching issues, we filtered off the catalyst after each cycle, washed with acetone, dried and then added into a fresh reaction mixture. It has been demonstrated that the solid state ^{31}P NMR (Figure 7a), Raman (Figure 7b), and HR-TEM (Figure 7c) results for the recovered catalyst are almost the same as those of the fresh one, indicating the stability and chemical composition of the catalyst. The aged $P_2W_{15}@Al_2O_3$ catalytic system can be reused for the oxidation of thioanisole, promoting the oxidation of sulfides to sulfoxides at least ten times without significant decrease of its catalytic efficiency (Figure 7d). Previously reported examples of catalytic oxidative efficiencies using sulfide substrates of various catalytic systems are summarized in Table S4. It is worth noting that the high efficiency and selectivity of the $P_2W_{15}@Al_2O_3$ catalyst along with the easy preparation in a single step, in less time and lower consumption of H_2O_2 during the catalytic conversion of the substrates (Table S4, entry 14) renders it an ideal candidate for larger scale applications.

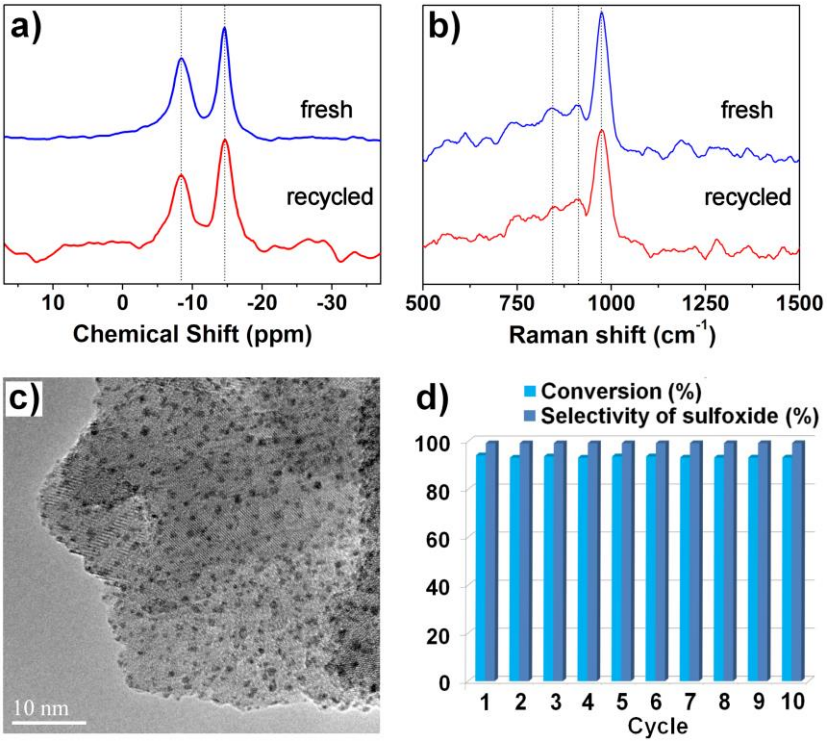

Figure 7. a) Solid state ^{31}P NMR, b) Raman spectra, and c) HRTEM images of the fresh $P_2W_{15}@Al_2O_3$ and the recycled $P_2W_{15}@Al_2O_3$, d) The recycling experiments for selective oxidation of sulfides to sulfoxides using the $P_2W_{15}@Al_2O_3$ as catalyst at 25 ^oC. Experimental conditions: thioanisole = 1 mmol, H_2O_2 =1 mmol, catalyst =2.5 μmol, CH_3OH = 200 μL, T = 25 ^oC, t = 35 min.

Conclusions

The immobilization of $\{P_2W_{15}\}$ onto spherical γ-Al_2O_3 particles results in the formation of a new heterogeneous catalyst, $P_2W_{15}@Al_2O_3$, where the strong covalent bond are formed between the $[\alpha\text{-}P_2W_{15}O_{56}]^{12-}$ clusters and the hydroxyl groups of the spherical γ-Al_2O_3 support inducing exceptional stability to the catalytic system. Moreover, the $\{P_2W_{15}\}$ is distributed uniformly onto the γ-Al_2O_3 surface as evidenced by HRTEM studies. Highly efficient oxygenation of thioethers can be achieved by the $P_2W_{15}@Al_2O_3$ in the presence of H_2O_2 with 99% selectivity of sulfoxides and 94% conversion in 35 min. The $P_2W_{15}@Al_2O_3$ can be separated easily by filtration and reused at least ten times without obvious decrease of the catalytic efficiency. The facile preparation, reusability, and efficacy of the heterogeneous $P_2W_{15}@Al_2O_3$ catalyst provides great potential for

industrial applications. Finally, the straightforward covalent attachment of the appropriate choice of the polyoxometalate core (architecture and composition) opens the door for further exploration and design of multi-functional catalytic materials tailored for specific applications. Our current research effort is focused on exploring the potential of the family of POM@Al_2O_3 catalysts for the development of chiral sulfoxides.

Methods

Chemicals and Materials: All chemicals were of analytical grade and were used as received without any further purification. Thioether compounds were purchased from Alfa Aesar. LiCl, HCl, KNO_3, HNO_3 and NaOH were purchased from Beijing Chemical Reagent Company (Beijing, China). Acetone, methanol, ethanol, acetonitrile and ethyl acetate were purchased from J&K Chemical Ltd. The spherical γ-Al_2O_3 was purchased from Shandong Benten Chemical Corporation. The deionized water from a Millipore water purification system was used throughout the experiments. $Na_{12}[\alpha\text{-}P_2W_{15}O_{56}]\cdot 24H_2O$ (P_2W_{15}) was prepared according to the published procedure.[25]

Instruments: Solid state NMR experiments were carried out at 10 kMHz for ^{31}P on a Bruker Avance 300M solid-state spectrometer equipped with a commercial 5mm MAS NMR probe. FT-IR spectra were collected in transmission mode using a JASCO FT-IR 410 spectrometer or a JASCO FT-IR 4100 spectrometer (wavenumbers (ν) are given in cm^{-1}; intensities are denoted as *wk* = weak, *sh* = sharp, *m* = medium, *br* = broad, *s* = strong). XRD measurements were performed in JCN UItimaIII X-ray diffraction. XPS data was received from the Thermo-Fisher scientific ESCALAB 250 X-ray photoelectron spectroscopy. TGA data was obtained using a DTG-60A analyzer of Shimadzu Corporation. TGA measurements were performed under Nitrogen atmosphere with a temperature increase of 10°C/min between 25 and 800°C. Laser Raman spectroscopy were obtained using a LabRAM ARAMIS Raman spectrometer. Scanning emission microscope (SEM) images were collected on a Zeiss Supra 55 VP field-emission scanning electron microscope. High-resolution transmission electron microscopy (HR-TEM) images were obtained with a JEOL JEM-3010 microscope operated at 300 kV. BET data were obtained using a Bei Shi De 3H-2000PS2 specific surface area and pore size analyzer. X-Ray Fluorescence

Spectrometer data were obtained using a XRF-1800 with 20 degree/min. The content of sulfides and sulfoxides were analyzed on an Agilent 7820A GC system using a 30 m 5% phenymethyl silicone capillary column with an ID of 0.32 mm and 0.25 mm coating (HP-5).

Synthesis of $P_2W_{15}@Al_2O_3$: The spherical γ-Al_2O_3 was activated at 900°C under atmospheric pressure for 24 h, then cooled down to room temperature in accordance to Cargnello et al.[45] In a reaction vessel, 1.66×10^{-4} mol of $Na_{12}[\alpha\text{-}P_2W_{15}O_{56}]\cdot 24H_2O$ were dissolved as a clear solution in 50 mL deionized water without CO_2, and then 1 g of spherical γ-Al_2O_3 was added to the solution. The pH of the solution was adjusted to 1.00 carefully by dropwise addition of 4 M HCl (aq). The reaction mixture was kept under stirring at room temperature for 1 hour and then heated at 90 °C for three hours.[46] The reaction mixture was cooled down to room temperature and the product was filtered and washed by 0.3 M of LiCl solution (100 mL × 3). The product was obtained after drying under vacuum oven at 60 °C for 24h.

Determination of IEP: The IEP (isoelectric points) value of γ-Al_2O_3 support was determined by a batch equilibration method as described in the literature.[47] 25 mg of spherical γ-Al_2O_3 support was dispersed in 25 ml of 0.1 M KNO_3 aqueous solution with vigorous stirring for 60 min. Six bottles of above solution were prepared and initial pH of each bottle was adjusted to 3, 4, 5, 6, 7, 8, 9, 10 and 11 using aqueous solution of HNO_3 or NaOH. The zeta potential of the solution was measured. The zeta potential value is plotted as a function of pH as presented in Figure S1. Finally, the pH_{IEP} value (ca. 8.6) of γ-Al_2O_3 support was determined at the point of Zeta Potential = 0.

Catalytic test: The oxidation reaction was carried out in a 25mL flask with magnetic stirring. The typical optimized procedure was the following: Thioanisole (1 mmol), H_2O_2 (1 mmol), CH_3OH (200 μL), $P_2W_{15}@Al_2O_3$ (2.5 μmol, the loading of P_2W_{15} on Al_2O_3: 9.98%) were added to the flask. The reaction time was counted after the addition of the catalyst (T = 25 °C, *t* = 35 min). The resulting products were extracted with diethyl ether and analyzed by GC. The yield was determined using reference standards. After completion of the reaction, the catalyst was recovered by filtration, washed with the acetone and dried in the oven.

1 Miras, H. N. *et al.* Engineering polyoxometalates with emergent properties. *Chemical Society Reviews* **41**, 7403-7430 (2012).

2 Pope, M. T. *In Borrás-Almenar, J. J., Coronado, E., Müller, A., and Pope M. T. Polyoxometalate Molecular Science*. 3-31 (2003).

3 Omwoma, S., Chen, W., Tsunashima, R. & Song, Y.-F. Recent advances on polyoxometalates intercalated layered double hydroxides: From synthetic approaches to functional material applications. *Coord. Chem. Rev.* **258-259**, 58-71, (2014).

4 Rives, V., Carriazo, D. & Martin, C. *A. Gill, S.A. Korili, R. Trujillano, M.A. Vicentè (Eds.), Pillared Clays and Related Catalysis*. 319-422 (Springer, 2010).

5 Bentaleb, F. *et al.* Efficiency of Polyoxometalate-Based Mesoporous Hybrids as Covalently Anchored Catalysts. *Inorganic chemistry* **54**, 7607-7616 (2015).

6 Liu, L., Wang, B., Du, Y. & Borgna, A. Supported $H_4SiW_{12}O_{40}/Al_2O_3$ solid acid catalysts for dehydration of glycerol to acrolein: Evolution of catalyst structure and performance with calcination temperature. *Applied Catalysis A: General* **489**, 32-41 (2015).

7 Armatas, G. S., Bilis, G. & Louloudi, M. Highly ordered mesoporous zirconia-polyoxometalate nanocomposite materials for catalytic oxidation of alkenes. *Journal of Materials Chemistry* **21**, 2997-3005 (2011).

8 Marleny Rodriguez-Albelo, L. *et al.* Zeolitic polyoxometalate-based metal− organic frameworks (Z-POMOFs): computational evaluation of hypothetical polymorphs and the successful targeted synthesis of the redox-active Z-POMOF1. *Journal of the American Chemical Society* **131**, 16078-16087 (2009).

9 Suárez-Guevara, J., Ruiz, V. & Gomez-Romero, P. Hybrid energy storage: high voltage aqueous supercapacitors based on activated carbon–phosphotungstate hybrid materials. *Journal of Materials Chemistry A* **2**, 1014-1021 (2014).

10 Li, B., Ma, W., Liu, J., Zuo, S. & Li, X. Preparation of MCM-41 incorporated with lacunary Keggin polyoxometalate and its catalytic performance in esterification. *Journal of colloid and interface science* **362**, 42-49 (2011).

11 Juan, J. C., Zhang, J. & Yarmo, M. A. 12-Tungstophosphoric acid supported on MCM-41 for esterification of fatty acid under solvent-free condition. *Journal of Molecular Catalysis A: Chemical* **267**, 265-271 (2007).

12 Zhang, Z. *et al.* Magnetically separable polyoxometalate catalyst for the oxidation of dibenzothiophene with H 2 O 2. *Journal of colloid and interface science* **360**, 189-194 (2011).

13 Armatas, G. S., Katsoulidis, A. P., Petrakis, D. E. & Pomonis, P. J. Synthesis and acidic catalytic properties of ordered mesoporous alumina–tungstophosphoric acid composites. *Journal of Materials Chemistry* **20**, 8631-8638 (2010).

14 Zhou, L., Wang, L., Zhang, S., Yan, R. & Diao, Y. Effect of vanadyl species in Keggin-type heteropoly catalysts in selective oxidation of methacrolein to methacrylic acid. *Journal of Catalysis* **329**, 431-440 (2015).

15 Potdar, H., Jun, K.-W., Bae, J. W., Kim, S.-M. & Lee, Y.-J. Synthesis of nano-sized porous γ-alumina powder via a precipitation/digestion route. *Applied Catalysis A: General* **321**, 109-116 (2007).

16 Lee, H. C. *et al.* Synthesis of nanostructured γ-alumina with a cationic surfactant and controlled amounts of water. *Microporous and mesoporous materials* **79**, 61-68 (2005).

17 Zhang, X., Zhang, F. & Chan, K.-Y. The synthesis of large mesopores alumina by microemulsion

templating, their characterization and properties as catalyst support. *Materials Letters* **58**, 2872-2877 (2004).

18 Mekasuwandumrong, O., Pavarajarn, V., Inoue, M. & Praserthdam, P. Preparation and phase transformation behavior of χ-alumina via solvothermal synthesis. *Materials chemistry and physics* **100**, 445-450 (2006).

19 Xu, B. *et al.* Synthesis of mesoporous alumina with highly thermal stability using glucose template in aqueous system. *Microporous and mesoporous materials* **91**, 293-295 (2006).

20 Aguado, J., Escola, J., Castro, M. & Paredes, B. Sol–gel synthesis of mesostructured γ-alumina templated by cationic surfactants. *Microporous and mesoporous materials* **83**, 181-192 (2005).

21 Farag, H., Whitehurst, D., Sakanishi, K. & Mochida, I. Carbon versus alumina as a support for Co–Mo catalysts reactivity towards HDS of dibenzothiophenes and diesel fuel. *Catalysis today* **50**, 9-17 (1999).

22 Maggi, R., Ballini, R., Sartori, G. & Sartorio, R. Basic alumina catalysed synthesis of substituted 2-amino-2-chromenes via three-component reaction. *Tetrahedron letters* **45**, 2297-2299 (2004).

23 Mulcahy, F. M., Fay, M. J., Proctor, A., Houalla, M. & Hercules, D. M. The adsorption of metal oxyanions on alumina. *Journal of Catalysis* **124**, 231-240 (1990).

24 Nag, N. K. A comparative study on the dispersion and carrier-catalyst interaction of molybdenum oxides supported on various oxides by electron spectroscopy for chemical analysis. *Journal of Physical Chemistry* **91**, 2324-2327 (1987).

25 Contant, R., Klemperer, W. G. & Yaghi, O. Potassium octadecatungstodiphosphates (V) and related lacunary compounds. *Inorganic Syntheses, Volume 27*, 104-111 (2007).

26 Izarova, N. V., Maksimovskaya, R. I., Willbold, S. & Kögerler, P. Tetrapalladium-Containing Polyoxotungstate [PdII4 (α-P2W15O56) 2] 16–: A Comparative Study. *Inorganic chemistry* **53**, 11778-11784 (2014).

27 Wachs, I. E. Raman and IR studies of surface metal oxide species on oxide supports: supported metal oxide catalysts. *Catalysis Today* **27**, 437-455 (1996).

28 Ross-Medgaarden, E. I. & Wachs, I. E. Structural determination of bulk and surface tungsten oxides with UV-vis diffuse reflectance spectroscopy and Raman spectroscopy. *The Journal of Physical Chemistry C* **111**, 15089-15099 (2007).

29 Tao, W., Li, Z., Pan, D., Nie, L. & Yao, S. Preparation, structure, and electrochemistry of a polypyrrole film doped with manganese (III)-substituted Dawson-type phosphopolyoxotungstate. *The Journal of Physical Chemistry B* **109**, 2666-2672 (2005).

30 Feng, C., Shang, H. & Liu, X. Photocatalysis of dinitrotoluene decomposition by $H_3PW_{12}O_{40}/TiO_2$ and H 4 SiW 12 O 40/TiO 2 prepared by a modified sol-gel synthesis and solvothermal treatment method. *Chinese Journal of Catalysis* **35**, 168-174 (2014).

31 Grünert, W. *et al.* A new facility for inert transfer of reactive samples to XPS equipment. *Journal of electron spectroscopy and related phenomena* **40**, 187-192 (1986).

32 Biloen, P. & Pott, G. X-ray photoelectron spectroscopy study of supported tungsten oxide. *Journal of Catalysis* **30**, 169-174 (1973).

33 Chowdari, B., Tan, K. & Chia, W. Raman and X-ray photoelectron spectroscopic studies of lithium phosphotungstate glasses. *Solid state ionics* **53**, 1172-1178 (1992).

34 Halada, G. & Clayton, C. Comparison of Mo–N and W–N synergism during passivation of stainless steel through x-ray photoelectron spectroscopy and electrochemical analysis. *Journal of Vacuum Science & Technology A* **11**, 2342-2347 (1993).

35 Guo, Y. *et al.* Microporous polyoxometalates $POMs/SiO_2$: synthesis and photocatalytic degradation of

aqueous organocholorine pesticides. *Chemistry of materials* **12**, 3501-3508 (2000).

36 Jørgensen, K. A. Transition-metal-catalyzed epoxidations. *Chemical Reviews* **89**, 431-458 (1989).

37 Meunier, B. Photosensitizing of biomolecules by porphyrins. *Chem Rev* **92**, 1411-1413 (1992).

38 Fernández, I. & Khiar, N. Recent developments in the synthesis and utilization of chiral sulfoxides. *Chemical reviews* **103**, 3651-3706 (2003).

39 Mikolajczyk, M., Drabowicz, J. & Kielbasinski, P. *Chiral sulfur reagents: applications in asymmetric and stereoselective synthesis*. Vol. 11 (CRC Press, 1997).

40 Phan, T. D., Kinch, M. A., Barker, J. E. & Ren, T. Highly efficient utilization of H_2O_2 for oxygenation of organic sulfides catalyzed by $[\gamma\text{-}SiW_{10}O_{34}(H_2O)_2]^{4-}$. *Tetrahedron letters* **46**, 397-400 (2005).

41 Gresley, N. M., Griffith, W. P., Laemmel, A. C., Nogueira, H. I. & Parkin, B. C. Studies on polyoxo and polyperoxo-metalates part 5: Peroxide-catalysed oxidations with heteropolyperoxo-tungstates and-molybdates. *Journal of Molecular Catalysis A: Chemical* **117**, 185-198 (1997).

42 Carraro, M. *et al.* Reactive ZrIV and HfIV Butterfly Peroxides on Polyoxometalate Surfaces: Bridging the Gap between Homogeneous and Heterogeneous Catalysis. *Chemistry-A European Journal* **17**, 8371-8378 (2011).

43 Kamata, K., Hirano, T., Kuzuya, S. & Mizuno, N. Hydrogen-bond-assisted epoxidation of homoallylic and allylic alcohols with hydrogen peroxide catalyzed by selenium-containing dinuclear peroxotungstate. *Journal of the American Chemical Society* **131**, 6997-7004 (2009).

44 Brégeault, J.-M. *et al.* From polyoxometalates to polyoxoperoxometalates and back again; potential applications. *Journal of Molecular Catalysis A: Chemical* **250**, 177-189 (2006).

45 Cargnello, M. *et al.* Exceptional activity for methane combustion over modular $Pd@CeO_2$ subunits on functionalized Al_2O_3. *Science* **337**, 713-717, (2012).

46 Kato, C. N., Kashiwagi, T., Unno, W., Nakagawa, M. & Uno, H. Syntheses and molecular structures of monomeric and hydrogen-bonded dimeric Dawson-type trialuminum-substituted polyoxotungstates derived under acidic and basic conditions. *Inorganic chemistry* **53**, 4824-4832, (2014).

47 Vidojkovic, S., Rodriguez-Santiago, V., Fedkin, M. V., Wesolowski, D. J. & Lvov, S. N. Electrophoretic mobility of magnetite particles in high temperature water. *Chemical Engineering Science* **66**, 4029-4035 (2011).

Acknowledgements

This research was supported by the National Basic Research Program of China (973 program, 2014CB932104), National Science Foundation of China (U1407127, U1507102), Fundamental Research Funds for the Central Universities (RC1302, YS1406). China Postdoctoral Science Foundation (2014M560878).

Additional Information

Supplementary information accompanies this paper at http://www.nature.com/scientificreports